How to determine the morphology of plasmonic nanocrystals without transmission electron microscopy?

Yann Battie, Irene Izquierdo-Lorenzo, Amandine Resano-Garcia, Aotmane En Naciri, Suzanna Akil, Pierre-Michel Adam, Safi Jradi

How to determine the morphology of plasmonic nanocrystals without transmission electron microscopy?

Yann Battie,[1]* Irene Izquierdo-Lorenzo,[2] Amandine Resano-Garcia,[1] Aotmane En Naciri,[1] Suzanna Akil,[1] Pierre Michel Adam,[2] Safi Jradi[2]

[1]*LCP-A2MC, Institut Jean Barriol, Université de Lorraine, 1 Bd Arago, 57070 Metz, France*

[2] *LNIO (CNRS UMR 6279), Université de Technologie de Troyes, 12 rue Marie Curie, 10010 Troyes, France*

*Corresponding author: yann.battie@univ-lorraine.fr

This paper reports the complete ellipsometric characterization of gold nanoparticles (NPs) embedded in a photoresist films. The effective dielectric function of nanocomposite films, as well as the shape distribution and the volume fraction of NPs are extracted from ellipsometric measurements by introducing an effective medium theory which takes into account the NP shape distribution and the intrinsic confinement effect. The redshift of the plasmon band as the gold volume fraction increases, is correlated to the evolution of NP shape distribution. This evolution is attributed to a competition between the nucleation and the coalescence of NPs. This unambiguously demonstrates that ellipsometry combined with a shape distributed effective medium theory, is a powerful alternative tool to transmission electron microscopy for the NP shape analysis.

1. Introduction

Plasmonic nanoparticles (NPs) embedded in polymer matrices are remarkable composites mainly for their unique optical properties[1-5], which lead to their application as filters, blackbody or re-usable optical sensors[6-11] but they have also proven enhanced conductivity[12-14], luminescence[15-16] and further worth as antibacterial agents[17-18]. Usually, these materials are characterized by UV-visible spectroscopy, as the plasmon resonance (SPR) of NPs provides qualitative information on the NP load, size, shape and distribution. However, in order to establish these parameters precisely, transmission electron microscopy (TEM) studies are required. Even then, the optical characterization of the material is limited using this technique, as it is blind to the elucidation of its refractive index.

Spectroscopic ellipsometry[19] is an indirect optical characterization tool based on the change of the polarization state of light after reflection on the sample. Ellipsometry requires an appropriate modeling to simultaneously determine the film thickness and dielectric constant. Ellipsometry was previously used to monitor the growth of silver NPs on a surface[20], in polymer[21-22] or mesoporous silica matrices[23]. However, classical effective medium theories, used to exploit ellipsometric data, only consider monodispersed NPs and could give erroneous results[24]. Persechini *et al.* have introduced the nanoparticle shape in effective medium theory to describe to exploit reflectance anisotropy spectroscopic measurements[25]. However, the authors consider monodispersed NPs. In addition, contrary to ellipsometry, reflectance anisotropy spectroscopic measurement is limited to oriented NPs. Recent advances in effective medium theory make it possible to take into account the influence of the NP size[26-27] or shape distribution[28-39] on the optical properties of films. An extension of effective medium theories was developed by Toudert *et al.*[28-29] to describe the optical properties of a collection of NPs distributed in shape and assembled into a 2 dimensional array. However, this model requires a preliminary

estimation of the pair correlation function of NPs by transmission electron microscopy. By considering mean field approximation, Bohren *et al.*[39] have introduced the NP shape distribution in the Maxwell Garnett theory. By assuming a low NP volume fraction, a spectral Bergman representation can be derived from this shape distributed effective medium theory (SDEMT)[34]. By combining mean field approximation and the Bruggeman theory, Goncharenko *et al.*[38] have investigated the influence of the NP shape distribution on their percolation threshold. However, these authors consider unphysical distributions such as uniform step-like shape distribution. SDEMT was successfully exploited to analyze the absorption spectra of colloids[31-32]. However, contrary to ellipsometry, absorption spectroscopy is not sensitive to the real part of the complex dielectric function of NPs.

This paper reports the first complete ellipsometric determination of the NP shape distribution of gold NPs embedded in a photoresist matrix. The aim behind the use of this resist is to develop metamaterials based on 3D metallic structures using 3D lithography. Based on a direct laser writing in a metallic precursor-loaded a photoresist solution, 3D metallic metamaterials can be obtained[40-41]. In this context, ellipsometry was used to get the optical properties and in particular the dielectric constant of gold NPs embedded in thin polymer films. It is interesting to note that in the present study, the NPs were thermally fabricated to obtain similar NP properties as in photo-patterned structure. Indeed, as we used a positive photoresist, the areas exposed to light are removed after the photolithographic step while the reduction of Au precursor and the growth of Au NPs inside the unexposed areas require a post annealing treatment. The ellipsometric data are analyzed by using the SDEMT model. In agreement with TEM, the NP shape estimated from ellipsometry evolves from spherical to non-spherical NPs as the gold concentration increases. This variation, which comes from a competition between the nucleation and the coalescence of NPs, has a significant impact on the complex dielectric function. It induces a red shift and a broadening of the plasmon resonance. This demonstrates that ellipsometry can

be used to simultaneously estimate the NP shape distribution and the complex dielectric function of nanocomposite films.

2. Materials and methods

A. Synthesis of the Au@AZ9260 composites

As a test material, we present a nanocomposite that includes Au NPs inside a well-known photosensitive pre-polymer which may still be used as two-photon lithography resist, as the similar composites prepared by Marques-Hueso *et al.*[42]. The Au NPs in the composite were generated *in situ*, reducing $HAuCl_4$ by the cresol novolac resist present in the AZ9260 commercial preparation. For each Au NP load level, weighted solutions of $HAuCl_4 \cdot 3H_2O$ in propyleneglycol monomethyl ether acetate (PGMEA) were added to the corresponding amount of commercial AZ9260. The mixtures were homogenized in an ultrasonic bath for one minute at room temperature. Immediately after preparation, they were spin coated over a silicon substrate at 5000 rpm for 60 s. Cleaned transparent glass substrates are also used for absorption spectroscopy measurements. Baking on hot plate for 8 minutes at 80 ºC followed by 2 minutes at 120 ºC evaporates all traces of solvent and activates the NP formation. While the AuNP load on the composite could be controlled by the amount of gold salt added to the polymer, the layer thickness was defined by the proportion of PGMEA. It was verified that a 70:30 proportion of PGMEA on AZ9260 at the former spin coating conditions led to uniform layers with thickness in the 150-250 nm range.

The gold load in each sample was expressed as the mass fraction of gold salt on the commercial AZ9260 as weighted for the solution preparation, ignoring further additional solvent. However, AZ9260 is specified to contain already a 60-65% wt. of solvents which are eliminated during soft bake. The relationship between the gold salt mass fraction and the final gold NP volume

fraction is shown in Table I. Uncertainties around 12% in the mass fraction are mainly due to the uncertainty in the polymer concentration in AZ9260, while an additional 8% uncertainty in the volume fraction is caused by the errors accumulated in the measurement of the polymer density.

Table I. Nominal gold mass and the corresponding nominal Au volume fractions for each formulation. The volume fraction of gold NPs deduced from ellipsometry is also reported.

For simplicity, the composites will be called by their nominal gold salt initial concentration.

Nominal $HAuCl_4$ concentration (% wt)	**Nominal f_{NP} (% vol)**	**f_{NP} from ellipsometry (% vol)**
5	0.6 ± 0.1	0.7± 0.1
10	1.0 ± 0.2	1.2± 0.1
20	2.2 ± 0.4	2.3± 0.8
40	6 ± 1	7±1
60	12 ± 2	11± 1

B. Characterization

Ellipsometric measurements were performed in the 0.59-4.43eV spectral range with a phase modulated ellipsometer (UVISEL, Horiba). The ellipsometric parameters Is, Ic were measured at three angles of incidence: 50°, 60° and 70°. These parameters depends on the ellipsometric angles Ψ and Δ:

$I_s = sin2\Psi sin\Delta$ (1)

$$I_c = sin2\Psi cos\Delta \text{ (2)}$$

TEM images are recorded with a Technai CM200 microscope operating at 200kV. To prepare TEM grids, the films are stripped off the substrate by scratching the samples with a razor blade. The film fragments are then deposited on a copper TEM grid. A downright microscope including a tungsten lamp for irradiation, a 10x (NA: 0.3) objective for collection in transmission mode and a Maya 2000pro UV-visible detector, was used for extinction spectra acquisition.

3. Shape distributed effective medium theory (SDEMT)

In the following, we consider a collection of spheroidal NPs distributed in shape and randomly oriented in a polymer matrix. This medium is considered as a homogeneous medium described by an effective dielectric function ε_{eff}. The random orientation of NPs suggests that this effective medium is isotrope. In mean field approximation, the spatial averages of electric <**E**> and displacement <**D**> fields in the material are the sum of two contributions[39]:

$$< \mathbf{E} >= (1-f) < \mathbf{E_m} > + f < \mathbf{E_{np}} >, \text{ (3)}$$

$$< \mathbf{D} >= (1-f)\varepsilon_m < \mathbf{E_m} > + f\varepsilon_{np} < \mathbf{E_{np}} >, \text{ (4)}$$

where f is the NPs volume fraction while <$\mathbf{E_m}$> and <$\mathbf{E_{np}}$> are the spatial average electric field inside the matrix and NPs, respectively. ε_{np} and ε_m are the complex dielectric function of NPs and the matrix, respectively. The effective dielectric function ε_{eff} is defined by:

$$< \mathbf{D} >= \varepsilon_{eff} < \mathbf{E} >. \text{ (5)}$$

In the quasi-static limit i.e. for NP size smaller than the wavelength, the field inside the matrix is proportional to the field inside NPs.

$$< \mathbf{E_m} >= \beta < \mathbf{E_{np}} >. (6)$$

The slope β is defined by[31]:

$$\beta = \frac{\varepsilon_m}{3} \int \int P(L_1, L_2) \sum_{i=1}^{3} \frac{1}{\varepsilon_m + L_i(\varepsilon_{np}(l) - \varepsilon_m)} dL_1 dL_2. (7)$$

The depolarization parameters (L_1, L_2, L_3) which only depend on the NP shape, vary in the 0-1 range and must respect the following sum rule:

$$1 = L_1 + L_2 + L_3. (8)$$

P(L_1, L_2) is the normalized distribution of NP depolarization factors. We assume that the depolarization parameters follow a Gaussian distribution[30-32]:

$$P(L_1, L_2) = Ce^{-0.5\left(\frac{(L_1-\bar{L}_1)^2}{\sigma_1^2} + \frac{(L_2-\bar{L}_2)^2}{\sigma_2^2} + \frac{(L_3-\bar{L}_3)^2}{\sigma_3^2}\right)}. (9)$$

Note that other distributions can be used. The distribution of NP depolarization factors is related to the NP shape distribution. $\bar{L_i}$ and σ_i are the mean value and standard deviation of L_i, respectively while C is a constant used to normalize the distribution. To make easier the interpretation, we adopt the Bohren convention[39]: $L_1 \leq L_2 \leq L_3$.

The effective dielectric function of a medium composed of ellipsoidal NPs embedded in a dielectric matrix can be calculated from equations (3)-(6):

$$\varepsilon_{eff} = \frac{(1-f)\varepsilon_m + f\varepsilon_{np}\beta}{(1-f) + f\beta}. (10)$$

Note that the volume fraction must be small enough to neglect the interaction between NPs[43-44]. The dielectric function of bulk Au (ε_{bulk})[45] related to the contribution of interband and

intraband transitions of bound and conduction electrons, respectively[46]. The interband transitions are described by the Drude dispersion law[46]. In a classical limit, intrinsic confinement occurs for NP size smaller than the mean free path of conduction electrons. By assuming that the intrinsic confinement only affects free electrons, the dielectric function of Au NPs can be deduced from:

$$\varepsilon_{np}(l) = \epsilon_{bulk} - \frac{\omega_p^2}{\omega(\omega+i\Gamma_0)} + \frac{\omega_p^2}{\omega\left(\omega+i\left(\Gamma_0+A\frac{v_f}{l}\right)\right)}, (11)$$

where ω is the photon energy and A a constant. ω_p=8.64eV, Γ_0=0.097 eV and v_f =1.4*10^6 m/s are the bulk plasma energy, the bulk electron damping and the Fermi velocity of free electrons, respectively. *l* is the mean value of NP size. The value of the constant A is still under debate and depends on the scattering scheme[46-47], the NP shape[47] and the chemical environment[48-50]. As example, in the case of spherical NPs in vacuum, an isotropic electron scattering leads to A=1 while A=0.75 for a Lambert cosine scattering law[47].

4. Results and discussion

Figure 1 shows typical TEM images of Au NP films and the corresponding diameter distributions measured over 300 NPs. In the following, the diameter is defined as the mean value between the smaller and larger dimensions of each NP. Since the thickness of the film chips obtained during the TEM grid preparation is not controlled, the concentration of NPs cannot be estimated by TEM. In first approximation, the NP diameter distribution follows a Gaussian distribution. Au5, Au10, and Au20 have similar NP diameter distributions centered close to 4 nm with 1 nm standard deviation. The Au40 diameter distribution has a slightly larger width estimated at 1.5 nm. On the other hand, the Au60 diameter distribution is drastically

broadened while its mean diameter is 3 times higher than the Au5 one. In all cases, the NP diameter is smaller than the 42 nm electron mean free path of bulk Au[46].

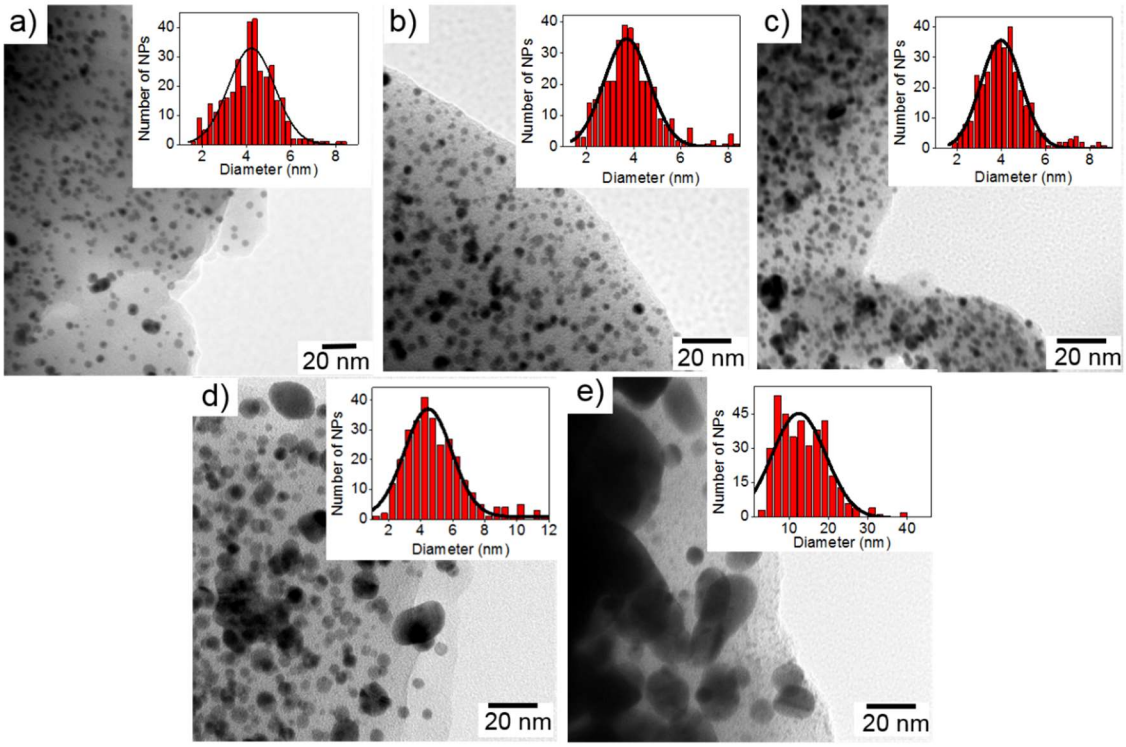

Figure 1. TEM images of (a) Au5, (b) Au10, (c) Au20, (d) Au40 and (e) Au60. In inset the corresponding NP diameter distributions.

The NPs aspect ratio distributions reported in Fig.2 enable a quantitative estimation of the NP shape distribution. In the following, the NP aspect ratio is defined as the ratio between the lower and the higher NP diameter. Au5, Au10 and Au20 mainly contain spherical NPs. However, the amount of spherical NPs tends to decrease from 86% to 30% as the gold precursor concentration increases from 5% to 60%. Indeed, as shown in the TEM image (Fig.1(e)), Au60 is mainly composed of elongated NPs which come from the coalescence of NPs. These NPs are randomly oriented inside the photoresist film.

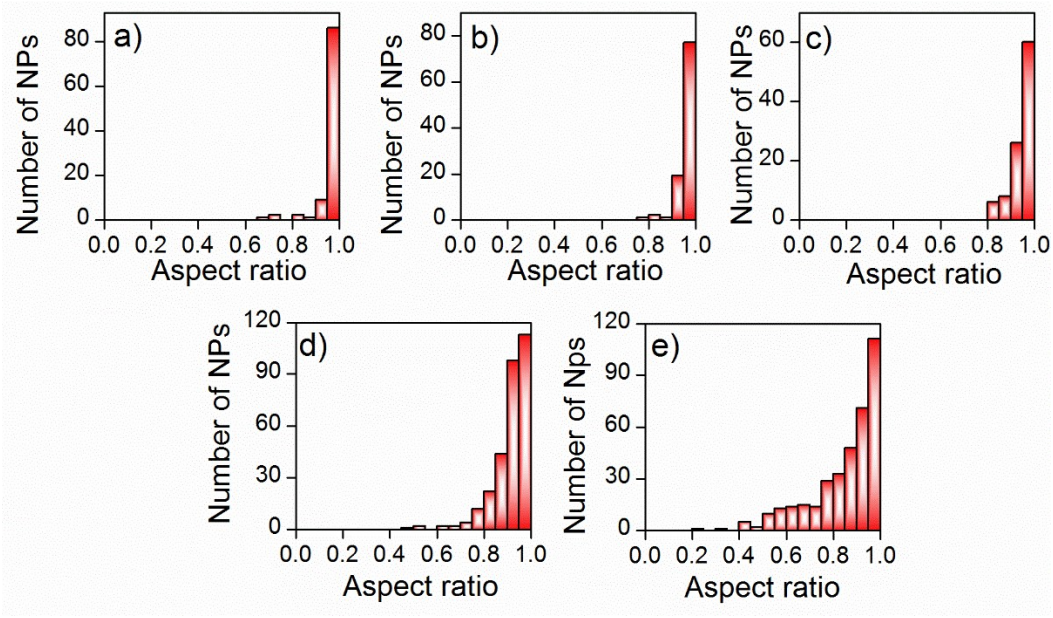

Figure 2. NP aspect ratio distribution of (a) Au5, (b) Au10, (c) Au20, (d) Au40 and (e) Au60.

The spectroscopic ellipsometric measurements of Au20 are illustrated in Fig.3. Similar spectra are obtained for other films (not shown). To extract optical properties of nanocomposite layers from ellipsometric data, an optical model must be introduced. This model consists of a silicon substrate covered with a photoresist film which contains Au NPs.

The optical properties of these films are described by an effective dielectric function calculated from equation (10). In agreement with the quasi-static approximation, the NP size deduced from TEM measurements is smaller than the wavelength. The dielectric function of the matrix ε_m is set to the value measured on a photoresist film without gold precursor. The transfer matrix formalism [19] is then used to calculate the ellipsometric parameters (I_s, I_c). The mean values ($\bar{L}_1$, $\bar{L}_2$) and standard deviations of (σ_1, σ_2, σ_3) of the distribution of depolarization factors, the NP volume fraction *f*, the ratio A/*l* and the film thickness have been simultaneously fitted by using the Levenberg-Marquard algorithm[51]. As shown in Figure 3, a good agreement is obtained between the experimental spectra and the calculated ones. The root mean square error between

the experimental and the simulated data does not exceed 0.06 for all films (spectra not shown), confirming the correctness of this model. Moreover, the correlation matrix (not shown) suggests that all free parameters are independent. The NP volume fractions deduced from ellipsometry (Table I) are close to the nominal values, suggesting that the gold salt is completely reduced during the heat treatment. In addition, the NP volume fraction is lower than 30%[52] confirming that the contribution of dipolar interactions between NPs can be neglected[46].

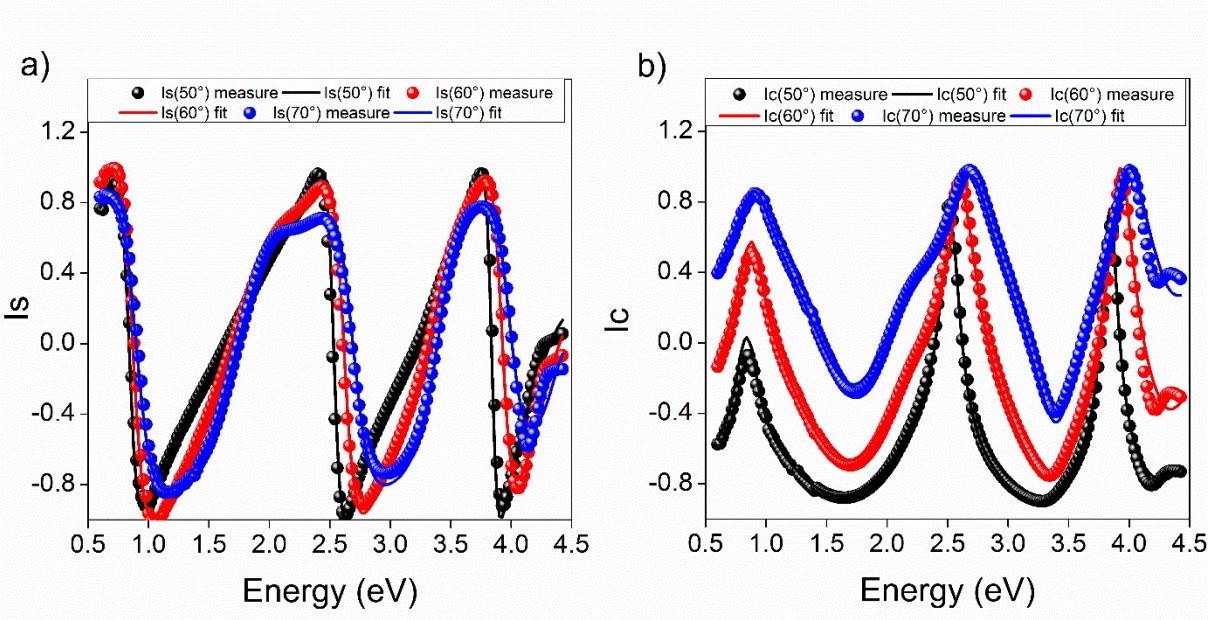

Figure 3. Measured and calculated (a) Is, (b) Ic ellipsometric spectra of Au20. The angles of incidence are 50°, 60° and 70°.

The distributions of NP depolarization factor P(L_1, L_2) deduced from ellipsometry are reported in Figure 4. Au5, Au10 and Au20 have narrow depolarization factor distribution centered close to (1/3, 1/3) suggesting that Au NPs are spherical for $HAuCl_4$ concentration lower than 20%. The distributions of depolarization factors are broadened for $HAuCl_4$ concentrations higher than 40%. Moreover, the mean values of depolarization factors deviate from that of spherical NPs.

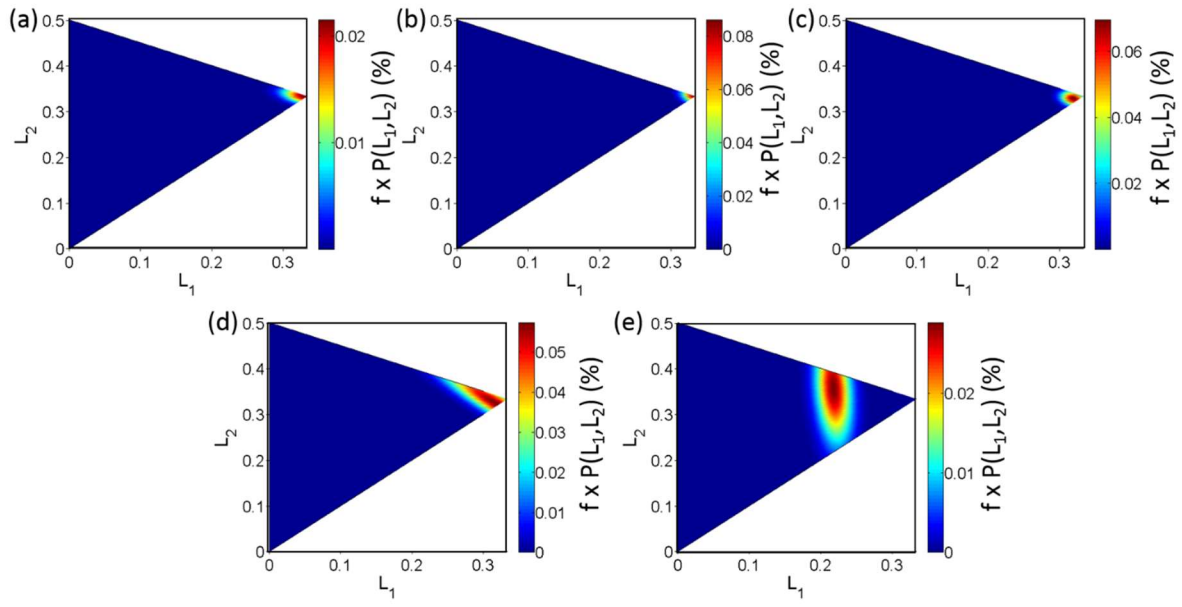

Figure 4. P(L_1,L_2) distribution of (a) Au5, (b) Au10, (c) Au20, (d) Au40 and (e) Au60.

The distribution of depolarization factor P(L_1,L_2) illustrated in Figure 4 can be converted into a distribution P(r_2,r_3) in aspect ratios of ellipsoidal NPs by applying the following space transformation[39]:

$$L_i = \frac{r_2 r_3}{2} \int_0^{+\infty} \frac{dq}{(q+r_i^2)\sqrt{\prod_{i=1}^{3}(q+r_i^2)}} \quad (12)$$

where $r_i = a_i/a_1$ (i=1,2,3) the aspect ratios of an ellipsoidal NP. a_1, a_2, a_3 are the length of principal axes of the ellipsoidal NP. To obtain a bijective space, the lengths of principal axes are sorted in the following order: $a_3 \leq a_2 \leq a_1$. The NP aspect ratios distributions are depicted in figure 5.

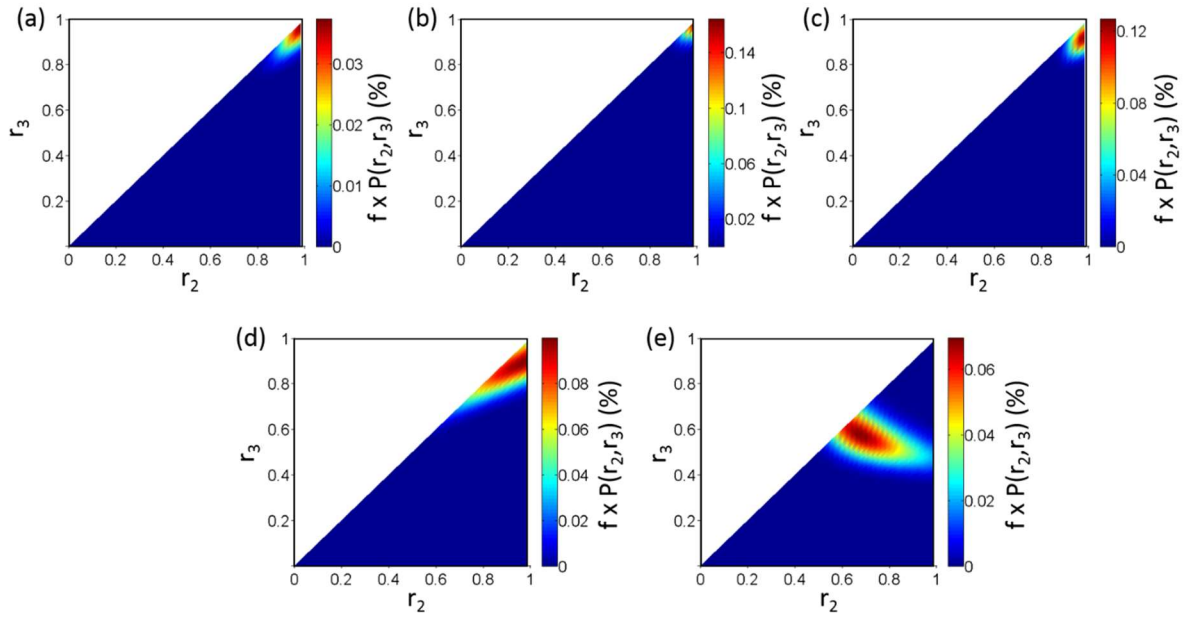

Figure 5. Distribution of NP aspect ratios P(r_2,r_3) of (a) Au5, (b) Au10, (c) Au20, (d) Au40 and (e) Au60.

In accordance with the NP aspect ratio distribution found by TEM (Fig.2), Au5, Au10 and Au20 are mainly composed of spherical NPs. Indeed, their aspect ratios r_2 and r_3 are close to 1. The distributions of aspect ratios are broadened for Au40 and Au60. In addition, the Au60 aspect ratio distribution is centered at the (0.68, 0.57) values confirming the non sphericity of NPs. This also suggests that the NP shape is close to prolate since the mean value of r_2 is close to the mean value of r_3. TEM measurements reveal that the nanoparticles aspect ratio is in the 0.4-1 range. However, a large number of NPs with an aspect ratio close to 1 is observed by TEM. TEM gives a two dimensional projection of NPs. Indeed, only one aspect ratio per NP can be measured by TEM. In other words, the aspect ratio estimated by TEM can be overestimated because non-spherical elongated nanoparticles could appear as closely spherical NPs, depending on their orientation.

To quantify the variations of NP shape distribution, we introduced the sphericity parameter P_s and the dispersity parameter D:

$$P_s = \sqrt{\sum_{i=1}^{3}\left(\overline{L}_i - \frac{1}{3}\right)^2}\ , (13)$$

$$D = \frac{1}{\sqrt{\sum_{i=1}^{3}\frac{1}{\sigma_i^2}}}\ . (14)$$

P_s is the Euclidian distance between the center of the depolarization factor distribution and the locus of spherical NPs. It varies in the 0-0.82 range. The sphericity parameter of monodispersed spherical NPs should be equal to 0. However, SDEMT does not take into account multipolar effects which appear for large NP radius[46]. To give a better sphericity criterion, spectra of spherical NPs simulated from Mie theory[39] are fitted with the SDEMT (not shown). We conclude that spherical NPs with a diameter smaller than 50 nm have a sphericity parameter smaller than 0.03. The dispersity parameter evaluates the width of the shape distribution. As example, monodispersed NPs have a D value close to 0. Figure 6 reports the variations of sphericity and dispersity with the $HAuCl_4$ concentration. The dispersity parameter remains approximately constant for $HAuCl_4$ concentration smaller than 20% while it drastically increases for higher concentrations. In addition, the sphericity parameters of Au5, Au10 and Au20 are lower than 0.03 confirming that these films are mainly composed of spherical NPs. The Au40 sphericity parameter is close to the spherical shape criterion threshold. However, it has a high dispersity parameter estimated at 0.019. The Au60 sphericity parameter and dispersity parameter are 0.15 and 0.065, respectively. In other words, Au40 and Au60 have broad NP shape distributions. Indeed, TEM images suggest that both films are composed of a mixture of spherical NPs, elongated NPs and faceted large NPs. The variations of the NP shape distribution with the Au concentration can be explained by considering two mechanisms: the nucleation and the coalescence of NPs. In a low concentration regime, the NP growth

mechanism is governed by the reduction of Au salt and the nucleation of isolated spherical NPs. A small rise of Au salt concentration increases the number of nucleation centers, i.e. the number of NPs, without changing their radius distribution. Then, the coalescence of NPs appears for a gold precursor concentration higher than 40%. This induces the growth of large non spherical NPs.

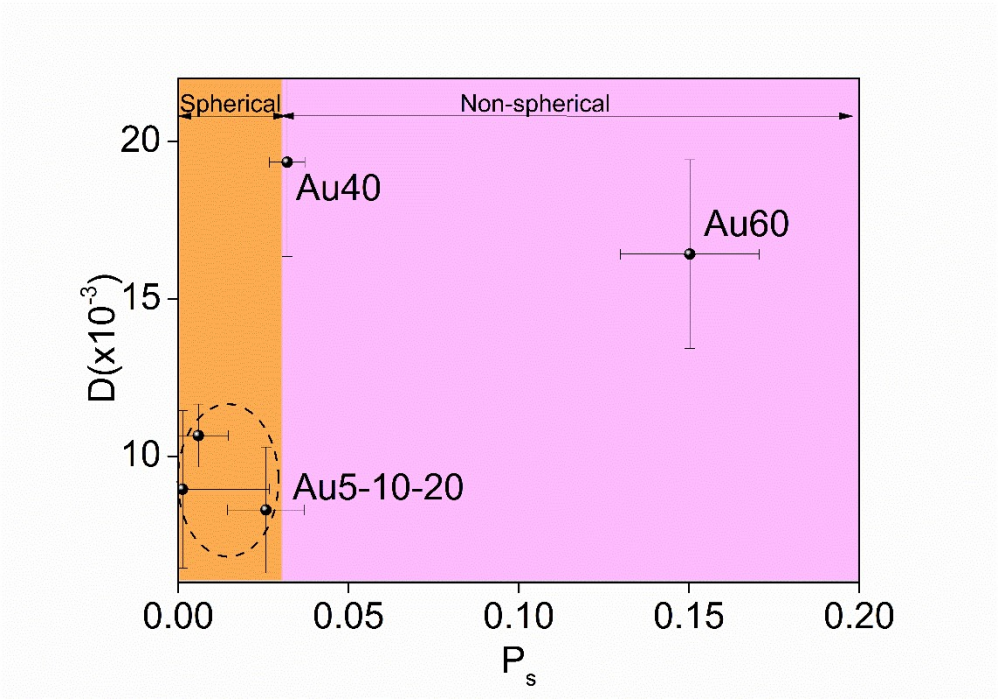

Figure 6. Dispersity parameter versus the sphericity parameter for each $HAuCl_4$ concentration

The NP mean radius obtained by TEM (Fig.1) is smaller than the 42 nm electron mean free path of Au[46]. In other words, the scattering of electrons on the NP surface limits their mean free path. This suggests that the constant A can be calculated from the product between the ellipsometric estimation of A/*l* and the NP mean radius deduced from TEM. Figure 7 reports the calculated A parameter as a function of the sphericity and dispersity parameters. The magnitude of the A error bars is calculated by taking into account the error on A/*l* deduced from the fitting procedure and the standard deviation of NP radius distribution obtained from TEM.

For a sphericity parameter smaller than 0.03, i.e. for nearly spherical NPs, the A parameter collapses to the 1.42 ±0.26 value. As reported by several authors[46-50], the A parameter of spherical NPs in vacuum or in air is smaller than 1. However, for embedded NPs, an energy transfer between the NP and its matrix can occur for a plasmon energy close to the adsorbate energy levels[48-50]. This chemical interface damping, which reflects the chemical and structural properties at the NP-matrix interface, damps the phase coherence of the collective oscillation. As example, Kreibig *et al.*[46,48-49] have reported a value A of 1.4 for silver NPs embedded in silica matrix. In other words, the chemical damping plays a major rule in the optical properties of small spherical NPs embedded in photoresist film. On the other end, Au40 and Au60 which have broad NP size and shape distributions, have A parameter larger than 2. As reported by Coronado *et al.*[47], the A parameter is shape and aspect ratio dependent. As example, the A parameter of oblate NPs in vacuum varies in the 0.25-1.7 range. Moreover, the high error bars of the A parameter of Au40 and Au60 are related to their broad NP size distributions. Indeed, the size distribution which can induce inhomogeneous broadening of the SPR bands, is not taken into account in SDEMT. In other words, the high A parameter value of Au40 and Au60 is due to their broad NP size and shape distributions and the deviation of the NP shape from spherical NPs.

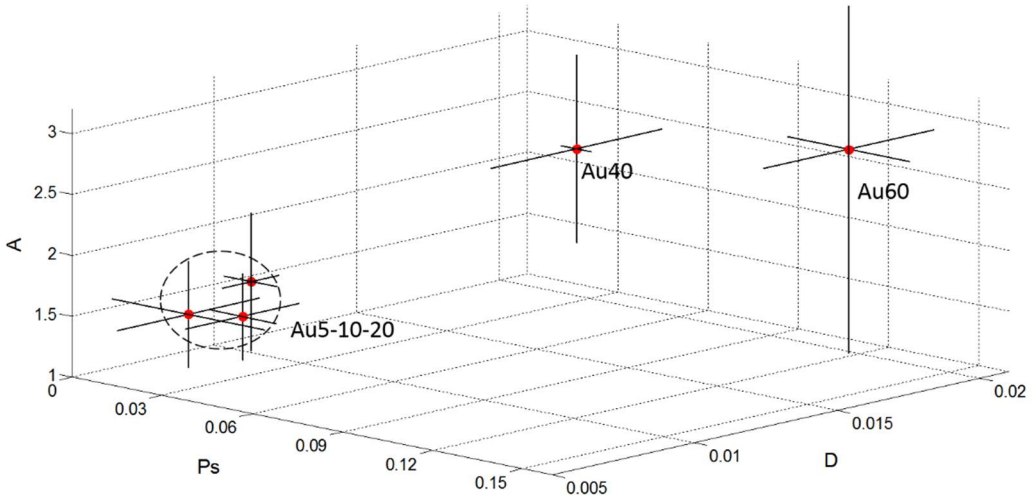

Figure 7. Influence of the sphericity and dispersity parameters on the value A.

The NP shape distribution has a strong influence on their optical properties. Figures 8(a)(b) show the real part and the imaginary part of the effective dielectric function of films. The effective absorption coefficients of the photoresist/Au NP films calculated from the effective dielectric functions and the normalized absorption measured by absorption spectroscopy are also reported in Fig.8(c)(d). Note that due to the random orientation of NPs, the Au NPs/photoresist film is described as an isotropic effective medium. The complex dielectric function of the photoresist matrix is also reported. The matrix is transparent below 3.6eV while it has a non-negligible absorption for higher energy. The contribution of 5d→6sp interband transitions of Au NPs is traduced by a nearly constant imaginary part of the effective dielectric function in the 2.7eV-4eV range which increases with the Au concentration. The imaginary part of dielectric function and the absorption coefficient exhibit a strong asymmetric SPR band located in the 2eV-2.5eV range. In accordance with the Kramers Kronig relations[53], a large variation of the real part of the effective dielectric function occurs close to the resonance. The absorption coefficient deduced from ellipsometry is in agreement with the normalized

absorption measured by absorption spectroscopy (Fig.8(c)) confirming the correctness of the ellipsometric model. The small differences between the spectra obtained by absorption spectroscopy and ellipsometry is due to the fact that both measurements are made on different samples. Indeed, contrary to ellipsometry, absorption measurement cannot be performed on non-transparent substrate. In addition, the determination of absorption coefficient from absorption spectroscopy requires the knowledge of film thickness and the losses, due to the reflection at each air/film and film/substrate interfaces, are not taken into account in absorption spectroscopy. Moreover, the complex dielectric function, which is a crucial parameter to design optical devices such as waveguides, or metamaterials cannot be extracted by absorption spectroscopy. Although the volume fractions are different, the dielectric functions of Au10 and Au20 are close together confirming that the polarization state of light is sufficiently sensitive to detect small variations of the complex dielectric function. The SPR energy of Au5, Au10 and Au20 is 2.25eV. In accordance with the Fröhlich relation[46], this band is assimilated to the SPR band of spherical NPs. The SPR band is redshifted from 2.25eV to 2eV while its full width at half maximum increases by 1.5 times when the Au precursor concentration evolves from 20% to 60%. Moreover, a shoulder attributed to the transversal SPR mode of nonspherical NPs is observed at 2.2-2.3eV in the effective absorption coefficient and the measured absorption spectra of Au60 (Fig.8(c)(d)). The SPR energy and bandwidth are mainly influenced by the mean value and the width of the depolarization factor distribution, respectively[31]. In order words, the high NP shape dispersity in Au40 or Au60 induces an inhomogeneous broadening of the plasmon band.

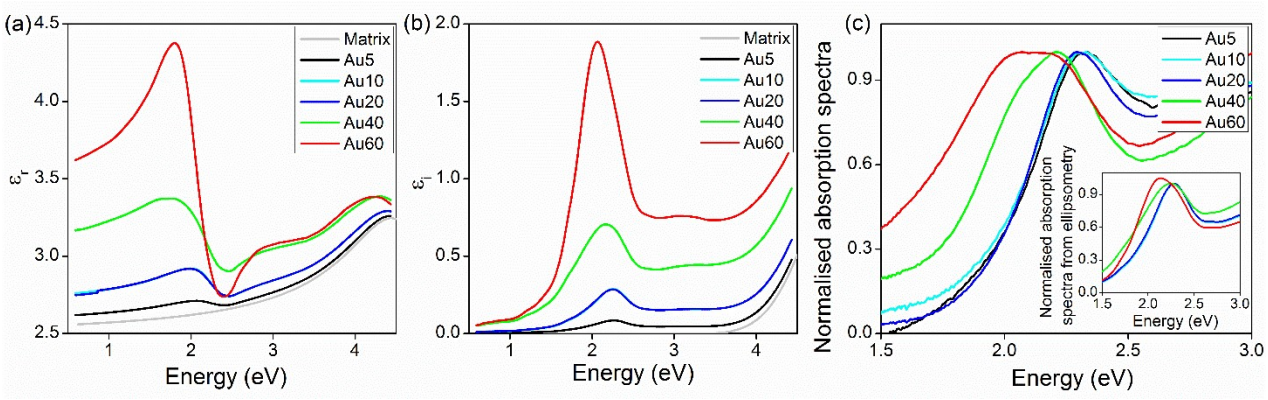

Figure 8. (a) Real part and (b) imaginary part of the effective dielectric function of Au NPs/photoresist films. The dielectric function of the photoresist matrix is also reported. (c) Normalised absorption spectra of films deposited on glass substrate measured by absorption spectroscopy. In inset, normalized effective absorption coefficient of the photoresist/Au NP films deduced from ellipsometry.

5. CONCLUSIONS

In summary, we have introduced an effective medium theory which takes into account the intrinsic confinement effect and the distribution of NPs shape. This theory has been used to analyze ellipsometric spectra recorded on photoresist films which contain Au NPs. The shape distributions and volume fraction are extracted from ellipsometric measurements. Contrary to TEM measurements, the NP shape distribution is obtained from a large number of NPs. Indeed, by considering the ellipsometric beam diameter, the film thickness and the NP volume fraction, we can conclude that the light beam probes approximately 10^{11} NPs. Moreover, contrary to TEM measurements, ellipsometry is a non-destructive technique which gives the dielectric function of nanocomposite film. Thus, we demonstrate that ellipsometry combined with SDEMT, is an inexpensive alternative for TEM to estimate the NPs shape distribution.

Acknowledgements

Financial support of the "Conseil régional Champagne-Ardenne", NanoMat (www.nanomat.eu) by the "Ministère de l'enseignement supérieur et de la recherche" is acknowledged.

References

[1]Qu, S.; Songa, Y.; Dub, C.; Wanga, Y.; Gaoa, Y.; Liua, S.; Lib, Y.; Zhu D. Nonlinear optical properties in three novel nanocomposites with gold nanoparticles. *Opt. Comm.* **2001**, 196, 317-323.

[2]Biswas, A.; Aktasa, O. C.; Kanzowa, J.; Saeeda, U.; Strunskusb, T.; Zaporojtchenkoa, V.; Faupela, F. Polymer-metal optical nanocomposites with tunable particle plasmon resonance prepared by vapor phase co-deposition. *Mater. Lett.* **2004**, 58, 1530-1534.

[3]Pacios, R.; Marcilla R.; Pozo-Gonzalo, C.; Pomposo, J. A.; Grande, H.; Aizpurua, J.; Mecerreyes, D. Combined electrochromic and plasmonic optical responses in conducting polymer/metal nanoparticle films. *J. Nanosci. Nanotechnol.* **2007**, 7, 2938-2941.

[4]Noguez, C. Surface plasmons on metal nanoparticles: the influence of shape and physical environment. *J. Phys. Chem. C* **2007**, 111, 3806-3819.

[5]Kinnan, M. K.; Kachan, S.; Simmons, C.K.; Chumanov G. Plasmon coupling in two-dimensional arrays of silver nanoparticles: I. effect of the dielectric medium. *J. Phys. Chem. C* **2009**, 113, 7079–7084.

[6]Aldeanueva-Potel, P.; Faoucher, E.; Alvarez-Puebla, R. A.; Liz-Marzán, L. M.; Brust, M. Recyclable molecular trapping and SERS detection in silver-Loaded agarose gels with Dynamic hot spots. *Anal. Chem.* **2009**, 81, 9233-9238.

[7]Gradess, R.; Abargues, R.; Habbou, A.; Canet-Ferrer, J.; Pedrueza, E.; Russell, A.; Valdés J. L. Martínez-Pastor, J. P. Localized surface plasmon resonance sensor based on Ag-PVA nanocomposite thin films. *J. Mater. Chem.* **2009**, 19, 9233-9240.

[8]Hedayati, M. K.; Javaherirahim, M.; Mozooni, B.; Abdelaziz, R.; Tavassolizadeh, A.; Chakravadhanula, V. S. K.; Zaporojtchenko, V.; Strunkus, T.; Faupel, F.; Elbahri, M. Design of a perfect black absorber at visible frequencies using plasmonic metamaterials. *Adv. Mater.* **2011**, 23, 5410-5414.

[9]Liu, Y.; Mills, E. N.; Composto, R. J. Tuning optical properties of gold nanorods in polymer films through thermal reshaping. *J. Mater. Chem.* **2009**, 19, 2704-2709.

[10]Pandey, S.; Goswami, G. K.; Nanda, K. K. Green synthesis of biopolymer-silver nanoparticle nanocomposite: An optical sensor for ammonia detection. *Int. J. Biol. Macromol.* **2012**, 51, 583-589.

[11]Kedem, O.; Vaskevich, A.; Rubinstein, I. Critical issues in localized plasmon sensing. *J. Phys. Chem. C* **2014**, 118, 8227–8244.

[12]Kuila, B. K.; Garai, A.; Nandi, A. K. Synthesis, optical, and electrical characterization of organically soluble silver nanoparticles and their poly(3-hexylthiophene) nanocomposites: Enhanced luminescence property in the nanocomposite thin films. *Chem. Mater.* **2007**, 19, 5443-5452.

[13]Reddy, K. R.; Lee, K. P.; Lee, Y.; Gopalan, A. I. Facile synthesis of conducting polymer-metal hybrid nanocomposite by in situ chemical oxidative polymerization with negatively charged metal nanoparticles. *Mater. Lett.* **2008**, 62, 1815-1818.

[14]Takele, H.; Schürmann, U.; Greve, H.; Paretkar, D.; Zaporojtchenko, V.; Faupel, F. Controlled growth of Au nanoparticles in co-evaporated metal/polymer composite films and their optical and electrical properties. *Eur. Phys. J.-Appl. Phys.* **2006**, 33, 83-89.

[15]Biteen, J.; Sweatlock, L. A.; Mertens, H.; Lewis, N. S.; Polman, A.; Atwater, H. A. Plasmon-enhanced photoluminescence of silicon quantum dots: simulation and experiment. *J. Phys. Chem. C* **2007**, 111, 13372–13377.

[16]Guzatov, D. V.; Vaschenko, S. V.; Stankevich, V. V.; Lunevich, A. Y.; Glukhov, Y. F; Gaponenko, S. V. Plasmonic enhancement of molecular fluorescence near silver nanoparticles: theory, modeling, and experiment. *J. Phys. Chem. C* **2012**, 116, 10723–10733.

[17]Kubacka, A.; Cerrada, M. L.; Serrano, C.; Fernández-García, M.; Ferrer, M.; Fernández-Garcia, M. Plasmonic Nanoparticle/Polymer Nanocomposites with Enhanced Photocatalytic Antimicrobial Properties. *J. Phys. Chem. C* **2009**, 113, 9182-9190.

[18]Tamboli, M. S.; Kulkarni, M. V.; Patil, R. H.; Gade, W. N.; Navale, S. C.; Kale, B. B. Nanowires of silver-polyaniline nanocomposite synthesized via in situ polymerization and its novel functionality as an antibacterial agent. *Colloid. Surface B* **2012**, 92, 35-41.

[19]Azzam, R. M. A.; Bashara, N. M. *Ellipsometry and Polarized Light*; Amsterdam: North-Holland Publishing Company, 1977.

[20]Oates, T. W. H.; Mücklich, A. Evolution of plasmon resonances during plasma deposition of silver nanoparticles. *Nanotechnology* **2005**, 16, 2606.

[21]Oates, T. W. H. ; Christalle, E. Real-time spectroscopic ellipsometry of silver nanoparticle formation in poly (vinyl alcohol) thin films. *J. Phys. Chem. C* **2007**, 111, 182-187.

[22]Oates, T. W. H. Real time spectroscopic ellipsometry of nanoparticle growth. *Appl. Phys. Lett.* **2006**, 88, 213115.

[23]Battie, Y.; Destouches, N.; Chassagneux, F.; Jamon, D.; Bois, L.; Moncoffre, N.; Toulhoat, N. Optical properties of silver nanoparticles thermally grown in a mesostructured hybrid silica film. *Opt. Mater. Express* **2011**, 1, 1019-1033.

[24]Keita, A. S.; Naciri, A. E. Size distribution dependence of the dielectric function of si quantum dots described by a modified Maxwell-Garnett formulation. *Phys. Rev. B* **2011**, 84, 125436.

[25] Persechini1, L.; Verre1, R.; McAlinden, N.; Wang, J J.; Ranjan, M.; Facsko, S.; Shvets, I. V.; McGilp J. F. An analytic approach to modeling the optical response of anisotropic nanoparticle arrays at surfaces and interfaces. *J. Phys.: Condens. Matter* **2014**, 26, 145302.

[26]Keita, A. S.; En Naciri, A.; Battie, Y.; Delachat, F.; Carrada, M.; Ferblantier, G.; Slaoui, A.; Determination of the optical properties and size dispersion of Si nanoparticles within a dielectric matrix by spectroscopic ellipsometry. *J. Appl. Phys.* **2014**, 116, 103520.

[27]Battie, Y.; Resano-Garcia, A.; Chaoui, N.; Zhang, Y.; En Naciri, A. Extended Maxwell-Garnett-Mie formulation applied to size dispersion of metallic nanoparticles embedded in host liquid matrix. *J. Chem. Phys.* **2014**, 140, 044705.

[28]Toudert, J.; Simonot, L.; Camelio, S.; Babonneau, D. Advanced optical effective medium modeling for a single layer of polydisperse ellipsoidal nanoparticles embedded in a homogeneous dielectric medium: Surface plasmon resonances. *Phys. Rev. B* **2012**, 86, 045415.

[29]Toudert, J.; Babonneau, D.; Simonot, L.; Camelio, S.; Girardeau, T. Quantitative modelling of the surface plasmon resonances of metal nanoclusters sandwiched between dielectric layers: the influence of nanocluster size, shape and organization. *Nanotechnology* **2008**, 19, 125709.

[30]Battie, Y.; En Naciri, A.; Chamorro, W.; Horwat, D. Generalized effective medium theory to extract the optical properties of two-dimensional nonspherical metallic nanoparticle layers. *J. Phys. Chem. C* **2014**, 118, 4899.

[31]Resano-Garcia, A.; Battie, Y.; En Naciri, A.; Akil, S.; Chaoui, N. Experimental and theoretical determination of the plasmonic responses and shape distribution of colloidal metallic nanoparticles. *J. Chem. Phys.* **2015**, **142**, 134108.

[32]Battie, Y.; Resano-Garcia, A.; En Naciri, A.; Akil, S.; Chaoui, N. Determination of morphological characteristics of metallic nanoparticles based on modified Maxwell-Garnett fitting of optical responses. *Appl. Phys. Lett.* **2015**, 107, 143104.

[33]Goncharenko, A. V.; Lozovski, V. Z.; Venger E. F. Effective dielectric response of a shape-distributed particle system. *J. Phys. Condens. Matter* **2001**, 13, 8217.

[34]Goncharenko, A.V. Spectral density function approach to homogenization of binary mixtures. *Chem. Phys. Lett.* **2004,** 400, 462-468.

[35]Goncharenko, A. V. Generalizations of the Bruggeman equation and a concept of shape-distributed particle composites. *Phys. Rev.* E **2003**, 68, 041108.

[36]Gao, L.; Li, Z. Effective medium approximation for two-component nonlinear composites with shape distribution. *J. Phys. Condens. Matter* **2003**, 15, 4397.

[37]Goncharenko, A. V.; Pinchuk, A. O. Broadband epsilon-near-zero composites made of metal nanospheroids. *Opt. Mater. Express* **2014**, 4, 1276-1286.

[38]Goncharenko, A. V.; Venger, E. F. Percolation threshold for Bruggeman composites. *Phys. Rev. E* **2004**, 70, 057102.

[39]Bohren, C. F.; Huffman, D. R. *Absorption and scattering by a sphere, in Absorption and Scattering of Light by Small Particles*; Wiley:Germany, 1998.

[40]Shukla, S.; Vidal, X;; Furlani, E. P.; Swihart, T. M.; Kim, K. T.; Yoon, Y. K.; Urbas, A.; Prasad, P. N. Subwavelength direct laser patterning of conductive gold nanostructures by simultaneous photopolymerization and photoreduction. *ACS Nano* **2011**, 5, 1947-1957.

[41]Ishikawa, A.; Tanaka, T. Two-Photon Fabrication of Three-Dimensional Metallic Nanostructures for Plasmonic Metamaterials. *J. Laser Micro Nanoen.* **2012**, 7, 11-15.

[42]Marques-Hueso, J.; Abargues, R.; Valdés, J. L.; Martínez-Pastor, J. P. Ag and Au/DNQ-novolac nanocomposites patternable by ultraviolet lithography: a fast route to plasmonic sensor microfabrication. *J. Mater. Chem.* **2010**, 20, 7436-7443.

[43]Hohenester, U.; Krenn, J. Surface plasmon resonances of single and coupled metallic nanoparticles: A boundary integral method approach. *Phys. Rev. B* **2005**, 72, 195429.

[44]Evlyukhin, A. B.; Reinhardt, C.; Urs Zywietz, U.; Chichkov, B. N. Collective resonances in metal nanoparticle arrays with dipole-quadrupole interactions. *Phys. Rev. B* **2012**, 85, 245411.

[45]Palik, E. D. *Handbook of Optical Constants of Solids*; Academic press handbook series: New York, 1985.

[46]Kreibig, U.; Vollmer, M. *Optical Properties of Metal Clusters*; Springer: Berlin, 1995.

[47]Coronado, E. A.; Schatz, G. C. Surface plasmon broadening for arbitrary shape nanoparticles: A geometrical probability approach. *J. Chem. Phys.* **2003**, 119, 3926-3934.

[48]Hövel, H.; Fritz, S.; Hilger, A.; Kreibig, U.; Vollmer, M. Width of cluster plasmon resonances: bulk dielectric functions and chemical interface damping. 1993 *Phys. Rev. B* **1993**, 48, 18178.

[49]Kreibig, U. Interface-induced dephasing of Mie plasmon polaritons. *Appl. Phys. B* **2008**, 93, 79-89.

[50]Charlé, K. P.; Frank, F.; Schulze, W. The optical properties of silver microcrystallites in dependance on size and the influence of the matrix environment. *Ber. Bunsenges. Phys. Chem.* **1984**, 88, 350.

[51]Levenberg, K. A Method for the solution of certain problems in least squares. *Q. Appl. Math.* **1944**, 2, 164-168.

[52]Myroshnychenko, V.; Rodrıguez-Fernandez, J.; Pastoriza-Santos, I. ; Funston, A. M.; Novo, C.; Mulvaney, P.; Liz-Marzan, L. M.; Garcıa de Abajo, F. J. Modelling the optical response of gold nanoparticles. *Chem. Soc. Rev.* **2008**, 37, 1792–1805.

[53]Kronig, R. D. L. On the theory of the dispersion of X-rays. *J Opt. Soc. Am.* **1926**, 12, 547-557.